5th Joint International Symposium on Deformation Monitoring (JISDM), 20-22 June 2022, Valencia, Spain
DOI: http://doi.org/10.4995/JISDM2022.2022.13853

Transferability of an estimation procedure for distance deviations of terrestrial laser scanners from laboratory to on-site conditions

Finn Linzer, Hans-Berndt Neuner

Department of Geodesy and Geoinformation, TU Wien, Wiedner Hauptstraße 8-10, 1040 Vienna, Austria, (finn.linzer@tuwien.ac.at; hans.neuner@geo.tuwien.ac.at)

Key words: *monitoring; laser scanning; systematic deviation; absolute distance; incidence angle (IA);* automation; robot operating system (ROS)

ABSTRACT

Employing terrestrial laser scanners (TLS) for geodetic deformation measurements requires attaining the highest possible accuracy. In this paper, we estimate the influence of varying incidence angles (IA) and materials on measurements regarding the distance component. Considering not only stochastic characteristics, the use of a scanning total station enables additionally the study of systematic distance deviations. By using the total station ocular, the device is brought into the local coordinate system of a laser tracker via position resection and intersection. The point cloud recording, with a Close-Range scanner, represents the reference. Due to transformation into a common coordinate system, defined by a laser tracker, a distance driven point comparison is possible. To test a large number of conditions an automated setup was developed. For each device, a suitable interface was implemented in the Robot Operating System. After the specimen has been set up, an automatic measurement can be performed for data acquisition. We can demonstrate that different building materials and varying IAs cause systematic distance deviations up to 3 mm magnitude. For measurement objects, this kind of correction must be considered, especially when the measurement configuration varies between measurement epochs. It can be demonstrated that the values and characteristics observed in the laboratory agree to those obtained on-site. However, the chosen approach thereby reveals previously unrecognized challenges that need to be considered for the use of TLS in high-accuracy deformation analysis.

I. INTRODUCTION

To detect deformations by using terrestrial laser scanners (TLS), it is necessary to further increase the accuracy with focus on the distance component. Sources of error can be divided into four groups: instrumental imperfection, atmospheric influences, scan geometry and object properties (Soudarissanane, 2016). To obtain a sophisticated model, systematic influences must be exposed, as they should no longer be confused with structural deformation.

The characteristics of the systematic distance deviations are not yet well understood. As it was stated by Zámečníková *et al.* (2014), varying the incidence angle (IA) alters the result. Following up on that methodology, the data acquisition was fully automated, so that research questions, such as the behavior with different materials, can be answered in even faster succession (Linzer *et al.*, 2021).

The methodology itself is driven by a straightforward distance comparison. Corresponding TLS- and reference measurements are examined in relation to a specific tilted specimen. The transformation $\mathcal{T}_{[6]}$ between the instruments in use is determined by a highly accurate network measurement. Figure 1 shows an overlay where the targeted points (51, 53, 61, 63) can be brought to a final correspondence by means of a spatial backward resection computation.

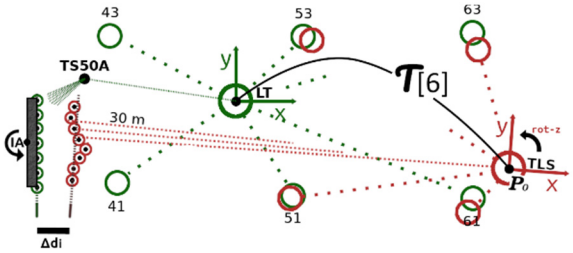

Figure 1. The transformation between TLS and LT system enable a direct comparison of the analyzed point clouds. The IA can set by a twistable specimen.

Ideally, after applying $\mathcal{T}_{[6]}$, point clouds of the TLS (in red) will be coincident with the points acquired by the reference (green). As laser radiation is affected by material properties and IA, deviations arise (Δdi).

As a superficial basis of laser radiation hitting various materials, "structure leads to properties" applies here (Shakelford, 2015). Following quantities can also be assumed to interfere: wavelength, distance, transmission, inhomogeneity, roughness, chem. composition, density, thickness, refraction, permeability, laser spot diameter and beam power. Thus, a penetration effect can be assumed for some materials, but can be ruled out for others. These findings must not be neglected when it comes to further developing of a potentially strong model for deformation analysis.

Furthermore, a stochastic description as a valid variance-covariance matrix (VCM) methodically has to meet the requirements of the elementary error model. In an on-site consideration a method was investigated in which especially the influences of atmosphere and geometry play a role (Kerekes and Schwieger, 2020). Wujanz *et al.* (2017) presented an intensity-based model that considered the reflectance properties of several laboratory setups. Based on the intensity value, a standard deviation of the distance component could be assigned to each point. To fill in the missing VCM entries Schmitz *et al.* (2021) made an effort, where a reference wall for TLS quality studies was established. The modeling of, for instance, the temporal influences on the geometry (*e.g.* daily influences) should ensure that deformations are not mistaken as device-specific phenomena. Through a large number of measurements and with a variety of instruments, the aim is to determine stochastic properties empirically.

In this paper, the transferability of results is examined on the basis of systematic deviations. If laboratory and on-sight results fit, we presume that subsequently laboratory findings have significance in outdoor applications as well. Due to a more complex setting, harsh conditions can obscure assumptions of results in a way not expected. If effects are similar, the sensitivity of deformation measurements can be increased by adapting and applying the given method to monitoring projects and its materials. The transfer to an outdoor structure, the historic aqueduct in Vienna, was achieved by using identical material that was available in the laboratory as well as on-site.

II. Sensors Automation and Data Transformation

In connection to a Leica LTD800 laser tracker, point clouds are acquired by a Close-Range scanner (T-Scan TS50A). Due to its high level of accuracy, these scans can be used as a reference (Table 1). The TLS results are acquired with three different Leica MS60 instruments, which, in addition to the usual tachymetric application, have a scanning function as a built-in feature. With an acquisition rate of up to 30.000 points per second, the MS60 is already capable for handling many geodetic applications. The three instruments are referred to as:

1) Loan1-MS60: A device loaned in March 2021.
2) Institute-MS60: This TLS belongs to the institute since May 2021.
3) Loan2-MS60: A device loaned in September 2021.

The methodology for measuring distance differences can be divided into four steps:

- First, a network measurement is carried out to define a common coordinate system for both devices. Identical points are targeted to, using a Corner Cube Reflector (CCR) for both systems. In the laboratory, the CCR is placed onto permanently installed consoles. For a network outside the laboratory, nests are spatially distributed and temporarily glued to the building facades.
- Thereafter specimens are examined in the laboratory for various IA. The materials chosen change in terms of roughness, reflection or permeability. On-Site, the IAs are realized by the geometric relationship towards the structure. However, the scan procedure always includes both the TLS and reference point clouds.
- Concluding control measurements must comply with the previous network measurement. It completes the acquisition and allows the detection of irregularities such as instability.
- At last, results can be evaluated using a scripted program.

Table 1. Properties of used devices

Parameter	Leica MS60	Leica LTD800 with T-Scan TS50A
Angular	0.3 mgon	0.6 mgon (LTD)
Distance	1 mm + 1.5 ppm	10 µm + 10 µm/m (IFM) and 3 µm (CCR)
with refl.		
Scanning	0.5 mm @ 25 m	80 µm + 3 µm/m (TS)
Laserspot	ca. 7 x 10 mm @30 m	4.5 mm (LTD, collimated)

After the transformation, the point clouds of both instruments are present in an overlapping arrangement – both with the origin at P_0. However, if differences in the distance component persist, those systematic influences can be revealed for any given setup by multiple straightforward distance comparisons. For any TLS point (red), a corresponding reference measurement is to be found (green). The assumed distance deviations Δdi arise and align closely on the line of sight. Therefore, matching point pairs are determined as nearest neighbors in polar space (Figure 2).

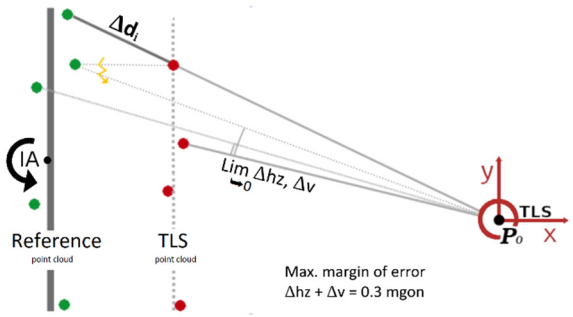

Figure 2. In the laboratory, the specimen is set to a certain IA. The corresponding point is assessed according to the deviation in Hz, V.

For measured distances of about 7 meters, the maximum angular difference allowed was set to 0.3 mgon. As the overall distance increases, the width may be reduced to remain a negligible impact on Δdi.

To the extent that the transformation parameters $\tau_{[6]}$ diverge, the distance deviation Δdi is also biased. A

Monte-Carlo-Simulation was carried out to estimate a priori accuracies with the values depicted in Table 1. The laboratory setup led to accuracy magnitudes of less than 0.1 mm in translation and about 0.5 mgon in orientation. In positioning, error proportions, which align to the line of site, fully affect the result of the distance component. An error on the z-axis orientation of 1 mgon would add about 0.15 mm to the error propagation of Δdi (Figure 2). Its actual influence depends on the IA and increases when the total distance becomes larger than the 7 meters assumed for this calculation.

A. *Robotized Method*

The effort required to determine the absolute distance deviations for a whole range of materials and incidence angles soon becomes overwhelming. Therefore, the automation of the data collection process was achieved. It facilitates an orderly structure and even makes it possible to answer emerging research questions in faster succession.

To adopt to the appropriate traverse path, a robotic arm is programmed with the Close-Range scanner. A setup was chosen in which a step angle motor controls the rotation of the plate around the vertical axis so that the rotation can be flexibly adjusted.

The estimation procedure is based on the Robot Operating System (ROS); an open source framework, which allows the modular design of complex geodetic systems (Linzer *et al.*, 2019; Rejchrt *et al.*, 2019). Individual function libraries are combined in packages for specific tasks. Preferred programming languages are C++ and Python. These packages enable the control and evaluation of certain devices. For the robot arm and the stepper motor, packages from the manufacturers were available, which simplified their integration considerably. For the TLS, the laser tracker and the Close-Range scanner, the packages first had to be developed by the RD EG at TU Wien. Other packages may contain task-related algorithms, which, for example, can be used to transform point clouds. Within the ROS environment, these packages can be easily exchanged, published and tested by anyone with respect to its own research. If another TLS is to be integrated, only the exchange of this single module is necessary. For future work, this principle allows us to focus on the essence of the task at hand. The sensor-processing packages are addressed via the appropriate interface:

- The total station acquires data via GeoCom (Leica, 2013).
- The laser tracker is addressed via the EmScon interface (Hexagon, 2019).
- The move-it package is used for a Universal Robot 5 robot arm (Universal Robotics, 2022).
- The rotation of the plate is adjusted by a dynamixel-stepper motor (ROBOTIS, 2022).

B. *Measurement campaigns and epochs*

A measurement campaign can extend over several measurement epochs, while the instrument's setup will remain. One epoch comprises the analysis of a certain material, which is examined in respect to different IAs.

1) Laboratory: The specimens are nearly planar plates, thus, when a certain position on the rotating table is approached, an approximately uniform IA is assumed. As the robotic arm reaches an area of about 40 cm x 40 cm, the plates are shaped alike. The measurement series of an epoch is set in a range from -60 to + 60 gon. Turning the specimen, scanning with the TLS and the recording of the Close-Range scanner takes about 8 minutes for each new IA. With angular increments of two gon, 61 IA are examined in total. With such configuration, one epoch takes about 8 hours.

In the laboratory, the distance to the specimen was modified from 7 m to 30 m at times. Respectively the instrument lies inside or outside the convex hull of consoles used for transformation. Still feasible in the laboratory, 30 m was chosen as a typical distance in TLS. The 7-meter arrangement refers to the distances to the aqueduct measured on-site.

2) On-Site: Due to the complexity of the setup, the automated point cloud acquisition can only be used in the laboratory. In the outdoor area, however, the environment must be captured manually. For this purpose, a structure was selected as an example for which the very same material is accessible, both, in the laboratory and in the outdoor area. For the historic aqueduct in Mauer, which still ensures Vienna's water supply today; Wien Wasser, the public utility authorities were able to provide the same type of bricks that are being used in ongoing renovation work. The surveyed wall is assembled from two kinds of bricks, which seem to differ only in color. The situation on-site allows a setup that permits observations of geometrically different IAs corresponding to the TLS standpoint.

III. INVESTIGATIONS UNDER LABORATORY CONDITIONS

In relation to the number of epochs and materials examined, conducting a campaign may take several days to complete. Therefore, climatically stable conditions in the laboratory must prevail. The devices are ideally in uninterrupted operation to avoid heating effects. After each epoch, the specimen is changed and the setup stability is repeatedly verified.

Two major campaigns were carried out in March and August 2021. Up to seven epochs and therefore transformations $\tau_{[6]}$ were measured. This allows an empirical consideration of the transformation parameter's precision (Table 2).

The translation's standard deviation of the campaign in March is rather high. This might be caused by the poor geometrical choice, as the instrument is located

outside all given console points. This arrangement is a compromise concerning the measuring distance. The results obtained in this way are yet satisfactory in terms of the absolute accuracy of the distance component. In contrast, the standard deviation of the rotation parameter obtained in the August campaign is raised. The network measurements reveal a slight increase of the rotation value between each epoch. An industrial tripod was used to achieve a comparable distance to the on-site measurements. It is less stable compared to the survey pillar used in March and maybe moved marginally. Adding the reported empirical transformation accuracy from Table 2 and the chosen margin of error for pairing, the total impact on Δdi will be in the range of 0.1 to 0.2 millimeters. In future projects, however, it must be taken care of even more intensively.

Table 2. Standard deviation of transformation parameters

$\mathcal{T}_{[6]}$ - campaign	March 2021	August 2021
Translation σx	71.18 µm	16.40 µm
Rotation σz	0.15 mgon	1.03 mgon
numb. of. tr.	7	6
convex hull	outside	inside
Distance	30 meter	7 meter
Device	Loan1-MS60	Institute-MS60

A. *Distance deviations and axis misalignment*

Once the acquisition and transformation is completed, the matching of the TLS- and reference-points can be carried out. Furthermore, the IA of the surface can be determined for each pair. At its origin, a flat surface is fitted into the reference point cloud, which corresponds approximately to the size of the laser spot. The orientation of this surface indicates the IA. In the following figures, each individual point represents a single computed distance deviation (as in Figure 3). In close proximity, more than 1000-point pairs are given for any observed IA. The distance comparison is determined in terms of the mean value and its standard deviation.

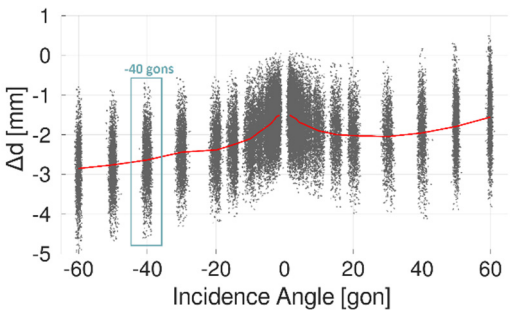

Figure 3. Distance Deviations of smooth granite for several IA (Institute-MS60).

The curve of a smooth granite plate was already examined in previous work and could be reproduced (compare Figure 3 to Linzer *et al.*, 2021). The range of recorded IA per lineup also represents the limitation of the resolving capability. It depends on the width and curvature of the specimen. For this case, a width of 2 - 3 gon can be accepted. Assuming planarity of the specimen, minor fluctuations will be omitted for the moment. One notes, that with respect to the orthogonal TLS axis, a slight horizontal inclination causes that the 0-gon situation cannot be observed (as in Figure 3). To validate the errors remained as random, the deviations obtained were tested against normal distribution. With the quantity and distribution shown exemplarily in Figure 4, for the IA at -40 gon a mean value of about 2.6 mm can be accepted.

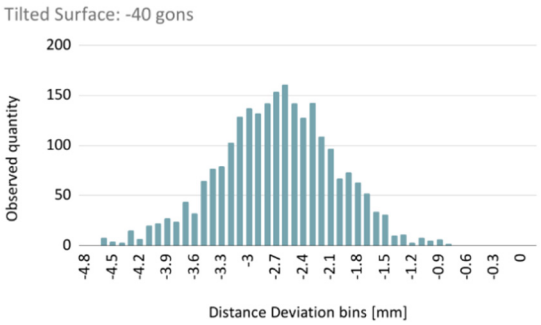

Figure 4. Distance Deviations of smooth granite for several IA (Institute-MS60).

The resulting standard deviation is about 0.6 mm for brick stones and the granite plate alike. This fits approximately the manufacturer's specifications for measurement noise in scanning mode (as in Table 1). The standard deviation of Δdi when scanning on different materials and IAs can be used to append the gained information to the VCM.

The present trend in the observed space of slightly more than 1 mm can be explained by an existing axis skew of the collimation and distance measurement axis (Zámečníková and Neuner, 2018). Ideally, there should be no such divergence, especially since its influence is growing with increasing distance. Such an axial skew was found for each of the three devices tested so far. The effect occurred both left- and right-skewed and was of varying magnitude. During the investigations of the past two years, it did not occur that this trend changed without external input. Only after a device was sent to the manufacturer for recalibration, it turned out that the collimation had been readjusted, but not fully eliminated. For the Loan2-MS60 device, which was investigated for outdoor use in the upcoming chapter, an influence could be determined which seems to be negligible due to a trend in the sub-millimeter range (Figure 11). To which extent a device shows such a trend can hardly be determined without the implemented methodology. Because the devices measure in only one position of the telescope, such effects are largely obscured in point clouds.

In addition to the smooth granite plate, Figure 5 shows the behavior of a shiny metal plate (blue). The curves have opposite characteristics, yet the reason for

this presence is not comprehensively researched yet. If the laser beam is incident on the smooth granite, the distance is measured about 2 millimeters too long. The ability of laser radiation to penetrate granite can be used as evidence. Specific characteristics can be found around 0 gon IA which must be related to the material properties. However, in the case of a metal plate, it is physically impossible for laser emissions to pass through (Shakelford, 2015). Thus, it appears that the diode might be overloaded by the reflective behavior of the metal plate below an IA with an absolute value of 15 gon. The time interval of the pulsed response could be disturbed. A possible argument for this could be that no measurement data can be obtained in the case of heavy directional reflection. The finding would be somewhat similar to the studies on some round-prisms, where it is also not advisable to target them at their direct angle of reflection (Lackner and Lienhart, 2016).

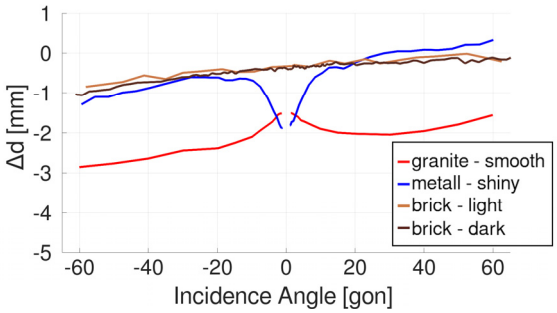

Figure 5. Distance Deviations of four different materials (Institute-MS60).

As the robotized setup is working appropriately, it is a straightforward process to evaluate further materials. To support the relevance of the findings presented, their transferability is examined in Section IV. For comparison, the same dark and light brownish bricks of which the aqueduct is built were brought to the laboratory as specimens. Opposed to granite or metal, both curves of the brick stones show no particular influence (Figure 5).

With such properties, they are particularly well qualified, thus any phenomena that may occur outdoors is not to be confused, in terms of distance deviation. The slightly different trend value might be plausible considering the transformation standard deviation discussed above. However, for some materials, there appears to be no obvious impact with varying IA. Besides, only a constant distance bias has to be reduced.

B. *Absolute Distance Deviation*

The trend results from the mechanical misalignment of the collimation and rangefinding axis. To highlight the material-dependent impact, its influence is eliminated by averaging two opposing IAs.

This also allows checking for the repeatability quality of results. The curves from two different devices and campaigns were stacked (Figure 6). These can be directly compared in the range of one to two tenths of a millimeter. To achieve similarity, the curves of the Loan1-MS60 instrument had to be reduced by an offset of 0.6 mm. Thus, it reveals the possible displacement among devices.

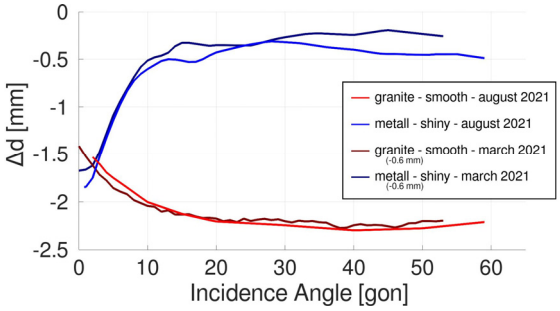

Figure 6. Distance Deviation: Instrument comparison (Institute and Loan1-MS60).

It is evident that an interaction of the laser radiation and the material generates deviations of several millimeters. Of all the materials that have been tested so far, the metal plate and granite stone show the clearest difference in direct comparison and mark the extreme cases according to the current findings. However, the extent to which this result depends on material properties or on the detection-capacity of the device can only be determined once results from any different TLS support these findings.

Figure 7 shows the curve progression of selected materials to illustrate the effects that can be assumed. If a diffuse reflection can be adopted for example due to roughness, occasionally no variation regarding the IA can be detected. This is also true for the observed wooden plate and roughened granite stone, although a possible penetration of the laser radiation could be detected as well. In many cases, applications regard deformations of concrete structures. Conforming our results (yellow-line) for such materials, an IA-specific correction seems negligible.

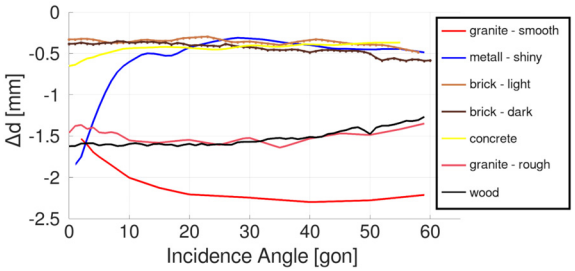

Figure 7. Absolute Distance Deviations of various materials (Institute-MS60).

C. *Intensities*

Intensities provide a potential insight into the underlying processes. Differences, such as surface characteristics can be revealed in relation to the IAs observed. Different levels of intensity can also be used to segment the given set of points or to apply a specific accuracy-model as proposed by Wujanz *et al.* (2017).

The distribution of the intensity (Figure 8) reveals a large gradient for the metal plate. However, the smooth granite plate and the measured concrete surface also show such an increase, albeit to a lesser extent. These materials can be assumed "smooth" in an immediate qualitative comparison. When running the fingertips over these materials, no pronounced irregularities can be perceived. Although concrete is similarly recognized as a smooth surface, the variations of the distance deviation is only weakly pronounced. The other materials reveal a pattern that can be attributed to diffuse back radiation. This loosely can be compared to a Lambertian radiator at different levels. Wood shows an increased level, but the overall interpretation remains difficult due to the lack of reference specifications so far.

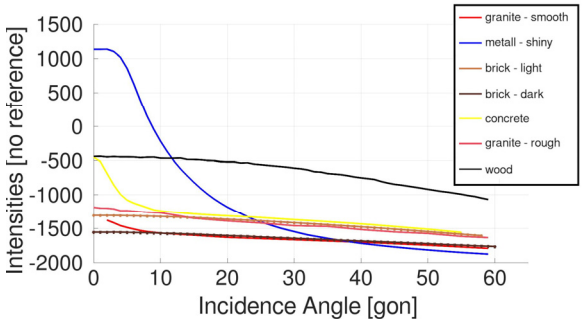

Figure 8. Absolute Intensities of various materials (Institute-MS60).

In the following chapter, the light and dark colored clinker bricks are examined in the field. These can be described as diffuse and not particularly pronounced. Nevertheless, as shown in Figure 8, both brick types can be distinguished based on IA and intensity (dotted lines), which may be relevant for segmentation efforts.

IV. Practical use under genuine conditions

As in the laboratory, the stability of the instruments used was ensured by multiple $\mathcal{T}_{[6]}$ network determinations. In addition, a concrete foundation was laid out to stabilize the laser tracker and the values of the circular bubbles of the TLS were monitored. As anticipated accuracy of the transformation, the values of the Monte-Carlo-Simulation from chapter II are to be assumed.

Unlike the empirical assessment, this statement is to be trusted as it is rather difficult to verify. In order to gain reliability, two measuring campaigns were evaluated. Campaign 1 and 2 were measured on 28th September and 09th November 2021. Figure 9 provides an impression of the conditions on-site. When examining both walls of the aqueduct, the IA is again determined by the orientation of the point cloud itself. Additionally the separation between brick fronts and gaps can be revealed by identifying points that are not part of a planar structure. Once the transformation is applied, the whole TLS point cloud had to be searched to find matching point pairs in the reference (as in Figure 2). Since both types of bricks adopt very similar values under laboratory conditions, no differentiation was initially made during the on-site evaluation. The determined curves should thus ideally lie within the range of the laboratory examination.

Figure 9. Instrument setup and left wall of aqueduct.

A. *Campaign 1: Eccentric location, two Devices*

Campaign 1 included the investigation of two scanning total stations, Institute- and Loan2-MS60 (Figure 9). Therefore, it allows the results to be reviewed against each other. In order to achieve a high IA, measurements were made eccentrically (Figure 10).

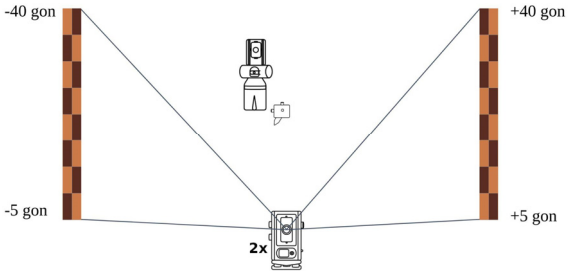

Figure 10. Schematic sketch of the eccentric setup (bird-eye).

1) Loan2-MS60: The blue curve from Figure 11 approximates the distance deviations measured on-sight. Compared to the laboratory data (brown), the overall data and axis offset could be reproduced. The on-sight and laboratory results of the Loan2-MS60 agree within a range of about one tenth of a millimeter. Furthermore, a similar order of magnitude could be determined for the offset, according to which all distance measurements are overshot by about 0.8 mm.

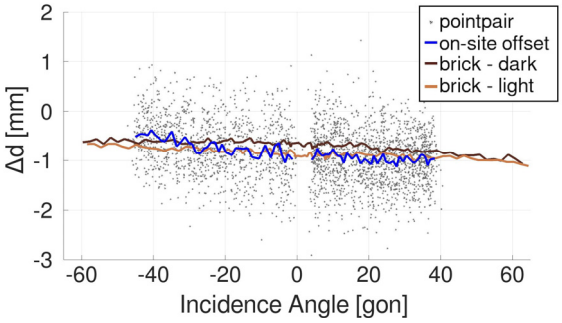

Figure 11. On-site offset compared to laboratory values (Loan2-MS60).

2) Institute-MS60: However, a general statement on the transferability is not yet permissible. Figure 12 reveals that it was not possible to obtain consistent data for the Institute-MS60. Therefore, a case distinction from device to device seems necessary. The data with negative IA (respectively the left wall) seems to match the overall deviation, but over the course of IAs, the laboratory examination fits poorly with a residue of about half a millimeter. Possibly, an unexpected and previously unobserved effect is revealed which does not follow any established pattern. In this evaluation, the left and right side of the wall can be clearly distinguished. This may occur as the walls are measured on very distinct parts of the TLS angular encoder.

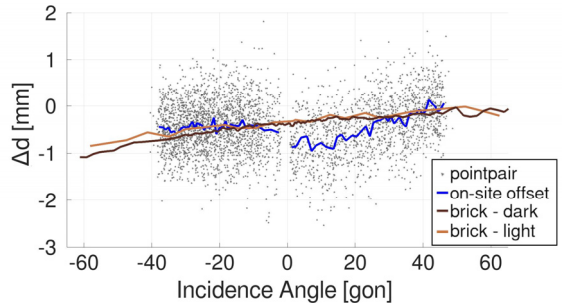

Figure 12. On-site offset compared to laboratory values (Institute-MS60).

B. *Campaign 2: Rerun eccentric measurement*

In Campaign 2 the Institute-MS60 was used only, in this case with the walls measured both eccentrically (Figure 10) and centric later on. An identical measurement setup was carried out in order to exclude external influences for the detected phenomenon. As Figure 13 shows, the phenomenon still occurred with similar characteristics. This justifies our finding, which clearly involves an external phenomenon that was out of our scope until yet. Since it is currently too early to identify a clear relationship, the results stand for themselves.

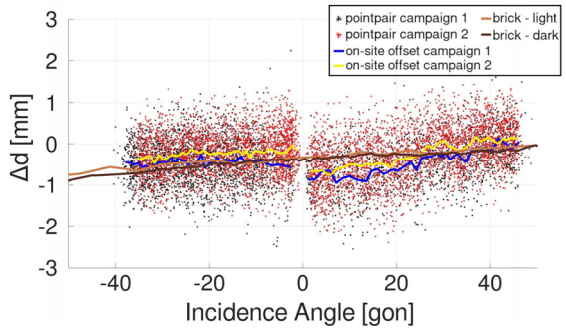

Figure 13. Two On-site offsets compared (Institute-MS60).

C. *Campaign 2: Centric measurement*

To gain further knowledge, the measurement setup was altered by placing the TLS right between the walls. This reduces the explorable range of IAs, but with positive and negative IAs respectively occurring on both walls for another result comparison (Figure 14). Using again the Institute-MS60, much more consistent results were obtained. In Figure 15, both sides of the wall show a progression that can be compared with the laboratory results. This might be because the angle encoder uses a section that covers an area that is not as affected. Thus, before a judgment can be made about its origin, we are seeking further investigations to determine its cause. For this purpose, a measurement setup is beneficial where the procedure can be realized over the full span of the angle encoder.

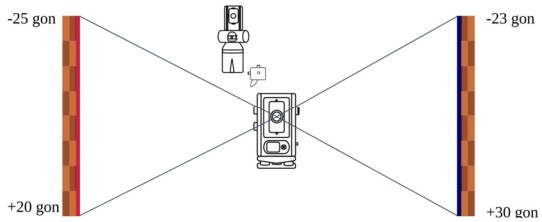

Figure 14. Schematic sketch of the centric setup, (bird-eye) (Institute-MS60 only).

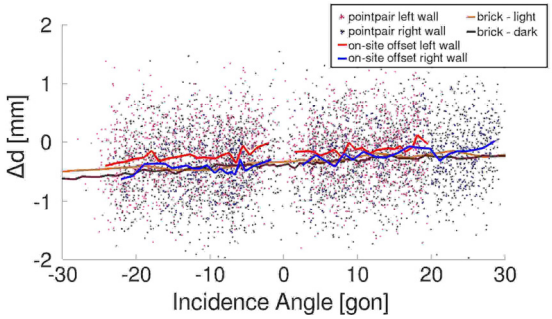

Figure 15. Centric setup: two walls offset comparison (Institute-MS60).

D. *Campaign 2: Centric measurement intensities*

A view on the intensities reveals another interesting aspect (Figure 16). Dark and light brown bricks can be distinguished based on intensity and IA. The range of light brown bricks is measured with an intensity roughly above -1400. Segmentation would be promising, since the areas overlap only marginally. However, the distance to both sides of the wall (blue and reddish) is approximately the same, yet there is a difference in the reflectance of about 200 units. These findings correspond to the laboratory examination, which matches regarding the characteristic, but not in terms of given magnitude. It must be noted that these intensity variations are as large as would be expected if the range to the object were shifted. Further investigations are necessary to clarify why these anomalies occur.

V. Conclusion

In a larger context, the present findings reveal that the inclusion of systematic distance deviation is crucial for TLS-driven deformation analysis. With regard to the material, millimeter accuracies can only be achieved if IA-dependent influences are taken into account.

Furthermore, the method makes it possible to detect the potential axis skew of the collimation and rangefinding axis.

The migration from the laboratory to the exterior is in agreement according to the values and characteristics observed. Moreover, a previously unrecognized phenomenon has been revealed and it is yet to be investigated how it relates to the deviation. As a first indication, the field-of-view and accordingly the angular encoder-usage differ between the inside and outside setup. Due to the narrow observation angle, with respect to the specimen in the laboratory, the mismatch had not been visible so far. It is of particular relevance that only for the Institute-MS60 such influences were uncovered.

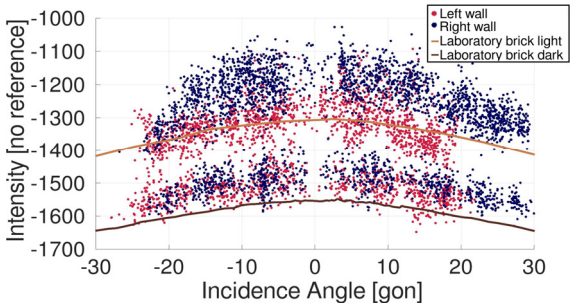

Figure 16. Centric setup: brick intensity comparison, campaign 2 (Institute-MS60).

Following up, the implementation of different types of TLS is planned. This poses a challenge in terms of the achievable transformation accuracy. Conventional 3D laser scanners cannot be positioned in the lower submillimeter range using current methods. It is beneficial that a recent paper by Janßen *et al.* (2021) indicates that the complete potential is not yet exploited. Taking not only the center of the targets but also their orientation into the registration adjustment is a step into the right direction.

In addition, a TLS that also includes the impulse answer would be of further interest. This could be used to uncover current questions about material dependences. The aim is to define more claims in a context that has general validity for laser radiation and its backscattering characteristics. In the next step, many more measurements are to be performed in a structured manner in order to make a statement about the roughness or the penetration effects. The robotized setup will support these efforts.

VI. Acknowledgements

We would like to thank Wien Wasser MA31 for their kind support and Leica Austria for the loaning of two MS60 TLS.

References

Hexagon (2019). emScon Reference Manual. Hexagon AB https://support.hexagonmi.com/s/article/What-is-emScon (retrieved 31.01.2022).

Janßen, J., Kuhlmann, H., and Holst, C. (2021). Target-based terrestrial laser scan registration extended by target orientation. *J. Appl. Geodesy*. (ahead of print). DOI: 10.1515/jag-2020-0030

Kerekes, G., and Schwieger, V. (2020). Elementary Error Model Applied to Terrestrial Laser Scanning Measurements: Study Case Arch Dam Kops. *Mathematics*. 2020; 8(4):593. DOI: 10.3390/math8040593

Lackner, S., and Lienhart, W. (2016). Impact of Prism Type and Prism Orientation on the Accuracy of Automated Total Station Measurements. Proceedings of the *Joint International Symposium on Deformation Monitoring (JISDM),* Vienna, Austria, 30 March–1 April 2016.

Leica (2013). GeoCOM Reference Manual. Leica Geosystems Heerbrugg (Switzerland).

Linzer, F., Barnefske, E., and Sternberg, H. (2019). Robot Operating System zur Steuerung eines Modularen Mobile-Mapping-Systems – Aufbau, Validierung und Anwendung. (peer-reviewed) avn Ausgabe 126 1-2, Wichmann Verlag im VDE VERLAG GMBH, Berlin.

Linzer F., Papčová M., and Neuner H. (2021). Quantification of Systematic Distance Deviations for Scanning Total Stations Using Robotic Applications. In: Kopáčik A., Kyrinovič P., Erdélyi J., Paar R., Marendić A. (eds) *Contributions to International Conferences on Engineering Surveying. Springer Proceedings in Earth and Environmental Sciences*. Springer. DOI: 10.1007/978-3-030-51953-7_8

Rejchrt, D., Thalmann, T., Ettlinger, A., and Neuner, H. (2019). Robot Operating System – A Modular and Flexible Framework for Geodetic Multi-Sensor Systems. avn Ausgabe 6-7, Wichmann Verlag-VDE VERLAG GMBH, Berlin.

ROBOTIS (2022). ROBOTIS Dynamixel SDK (Protocol1.0/2.0) http://wiki.ros.org/dynamixel_sdk (retrieved 31.01.2022)

Schmitz, B., Kuhlmann, H., and Holst, C., (2021). Deformation analysis of a reference wall towards the uncertainty investigation of terrestrial laser scanners. *J. Appl. Geodesy 15* (3), pp. 189–206.

Shackelford, J.F. (2015). *Introduction to Materials Science for Engineers*. Pearson Education Limited. University of California, Davis.

Soudarissanane, S.S. (2016). *The Geometry of Terrestrial Laser Scanning-identification of Errors, Modeling and Mitigation of Scanning Geometry*. Ph.D. Thesis, Technical University of Delft, The Netherlands.

Universal Robots (2022). Universal_Robots_ROS_Driver. http://wiki.ros.org/ur_robot_driver (retrieved 31.01.2022)

Wujanz, D., Burger, M., Mettenleiter, M., and Neitzel, F. (2017). An intensity-based stochastic model for terrestrial laser scanners. *ISPRS Journal of Photogrammetry and Remote Sensing*, 125, pp. 146-155.

Zámečníková, M., Wieser, A., Woschitz, H., and Ressl, C. (2014). Influence of surface reflectivity on reflectorless electronic distance measurement and terrestrial laser scanning. *Journal of Applied Geodesy*, 8(4), pp. 311-326.

Zámečníková, M., and Neuner, H. (2018). Methods for quantification of systematic distance deviations under incidence angle with scanning total stations. *ISPRS Journal of Photogrammetry and Remote Sensing*, 144, pp. 268 - 284.